CHEMIJA
2023. Vol. 34. No. 1. P. 32–40

ISSN 0235-7216 eISSN 2424-4538
DOI: https://doi.org/10.6001/chemija.2023.34.1.4

Three-dimensional Au(NiMo)/Ti catalysts for efficient oxygen evolution reaction

Sukomol Barua,

Aldona Balčiūnaitė*,

Jūratė Vaičiūnienė,

Loreta Tamašauskaitė-Tamašiūnaitė,

Eugenijus Norkus

Department of Catalysis,
Center for Physical Sciences
and Technology (FTMC),
3 Saulėtekio Avenue,
10257 Vilnius, Lithuania

In this study, three-dimensional gold-nickel-molybdenum (Au(NiMo)) catalysts have been studied as catalysts for the oxygen evolution reaction (OER). The catalysts have been deposited on a titanium surface using electroplating and galvanic displacement techniques. The modification of NiMo with a low amount of Au crystallites in a range of 1.2–5.2 $\mu g_{Au} cm^{-2}$ results in enhanced activity for OER in the alkaline medium compared to respective binary un-modified NiMo catalysts. The current densities for OER increase ca.1.2–7.3 and 1.3–5.1 times with an increase in temperature from 25 up to 75°C using the prepared 3D binary NiMo/Ti and Au(NiMo)/Ti catalysts, respectively.

Keywords: gold, nickel, molybdenum, three-dimensional catalysts, oxygen evolution reaction

INTRODUCTION

To address the ever-increasing energy demands and rapid depletion of fossil fuels and, at the same time, global warming and environmental emission, it is urgently important to exploit more and more clean and renewable alternative energy resources, e.g. solar, wind, geothermal energy, and bioenergy for a sustainable world. Research has shown that among those above-mentioned renewable fuels, hydrogen, the most abundant element on earth, can also be considered to be the most efficient main medium for energy storage in the future due to its excellent energy conversion efficiency, higher gravimetric energy density than gasoline (120 vs 44 MJ kg^{-1}), eco-friendliness, high-energy density, recyclability, as well as zero-emission of greenhouse gases [1–5].

Electrocatalytic water splitting has gained much research interest as one of the most promising methods for hydrogen production, as high pure hydrogen can be produced by electrochemical water splitting as an environment-friendly method [6, 7]. The electrochemical water splitting incorporates two half-reactions, namely the hydrogen evolution reaction (HER) and oxygen evolution reaction (OER) on the cathode and anode, respectively. Compared to HER, OER is the main bottleneck for electrocatalytic water splitting due to its dual influence of sluggish reaction kinetics with multiple proton-couple electron transfer reactions and thermodynamics. As water electrolysis is thermodynamically hindered at standard temperature and pressure and more potential is required in addition to the standard thermodynamic potential (1.23 V), it is necessary to fabricate efficient catalysts for OER to overcome the resistance and barriers of hydrogen production by OER overpotentials. In this scenario, material selection and design are the key factors for exploring high-active electrocatalysts substantiating their cost, stability, efficiency and earth-abundance [8–11].

As it is well established that water electrolysis in acidic electrolytes has higher energy efficiency and production rate compared to alkaline electrolytes, albeit the harsh corrosive acidic environment

* Corresponding author. Email: aldona.balciunaite@ftmc.lt

allows some noble metal-based catalysts only for both electrodes. At present, platinum (Pt) is the benchmark electrocatalyst for HER [12] and noble metals iridium (Ir), ruthenium (Ru) and their oxides (IrO_2 and RuO_2) have been regarded as promising excellent electrocatalysts for OER [13, 14], but their high production costs and low reserve limit the industrial application of noble metal catalysts for electrocatalytic water splitting. Therefore, due to the less corrosion ability of alkali, researchers have unveiled the engineering of non-noble metal electrocatalysts with a high activity and durability, and a low cost in recent years to promote the industrial development of alkaline water splitting.

In recent decades, researchers have developed several reaction mechanisms, such as the adsorbate evolution mechanism (AEM) [15] and lattice oxygen oxidation mechanism (LOM) [16], to fundamentally understand the reaction mechanisms and find the origin of the reaction overpotential at the active site of different materials. Using these discovered mechanisms as the guidelines, it is possible to design more efficient OER electrocatalysts by increasing the exposure of electrochemically active sites by reducing the particle size, engineering morphology of the catalyst, and promoting the surface reconstruction of the catalysts into the active species [17].

The OER mechanism involves the breaking of the O–H bond and the formation of the O–O bond and changes according to the pH of the electrolyte. In alkaline electrolytes, oxygen molecules are produced by the conversion of the OH^- through four-electron transfer steps. The mechanism of OER has been shown in Eqs. (1)–(5) for the alkaline medium [18–19]:

$$OH^- + {}^* \rightarrow OH^* + e^-, \quad (1)$$

$$OH^* + OH^- \rightarrow O^* + H_2O + e^-, \quad (2)$$

$$2O^* \rightarrow 2^* + O_2(g), \quad (3)$$

$$O^* + OH^- \rightarrow OOH^* + e^-, \quad (4)$$

$$OOH^* + OH^- \rightarrow {}^* + O_2(g) + H_2O(l) + e^-. \quad (5)$$

The total response is the following:

$$4OH^- \rightarrow 2H_2O(l) + O_2(g) + 4e^-.$$

Undoubtedly, over the past years, abundant low-cost transition metals on the earth (Ni, Fe, Mo, Co, Mn, Cu, etc.), their compounds and alloys with different elemental compositions have gained extensive attention as OER electrocatalysts to replace noble IrO_2 and RuO_2 electrodes. These electrocatalysts include monometallic [20, 21], bimetallic [22, 23] and trimetallic [24–26] transition metals as well as their carbides [27–29], nitrides [27, 30, 31], phosphides [32–34], sulphides [35, 36], etc. Studies revealed that in order to act as an electrocatalyst with an excellent electrocatalytic activity, the electrode must have a high surface active area as well as a high intrinsic electrocatalytic activity along with durability. The intrinsic electrocatalytic activity can be achieved by alloying various transition metals instead of using pure metal(s) and the electrochemically active surface area can be enhanced by fabricating different nanostructures such as nanowires [37, 38] nanosheets [4, 33, 39], nanocones [40], nanostars [9], etc. Other studies have demonstrated that binary, ternary and multinary alloying of transition metals such as Ni–Co [41], Ni–Mn [42], Mn–Co–Ni [43], Ni–Fe–Mo–Cu [44], etc. exhibit improved electrocatalytic activity for water splitting in different compositions. Among these transition metals, nickel can be considered to be an excellent candidate as an electrocatalyst because of its less free energy to absorb hydrogen and Ni–Mo_2C-embedded N-doped carbon nanofibers (Ni/Mo_2C–NCNFs) demonstrated as an excellent bifunctional electrocatalyst for overall water splitting delivering low overpotentials of 143 mV for HER and 288 mV for OER to attain current density of 10 mA cm^{-2} [45]. The synergistic effect between Ni and Mo is noteworthy here as the hydrogen binding energy (HBE) between Ni and H is slightly weaker, whereas it is stronger enough between Mo_2C and H. Thus, the HBE can be controlled to a relatively moderate value by chemically coupling Ni and Mo_2C, which could contribute to balance the thermodynamics between hydrogen adsorption and desorption [45, 46]. Nickel molybdenum nitride nanorods grown on Ni foam (Ni_{foam}@Ni–$Ni_{0.2}Mo_{0.8}N$) exhibit an excellent electrocatalytic performance in 1.0 M KOH with low overpotentials of 15 and 218 mV for HER and OER, respectively, at a current density of 10 mA cm^{-2} [31]. Furthermore, a unique fabrication of Ni–Mo nanostars by the electrochemical deposition method also resulted in an excellent

electrocatalytic behaviour where a minimum value of 60 mV and 225 mV overpotential were required for generating the current density of 10 $mAcm^{-2}$ in the HER and OER process, respectively, in the alkaline medium (1.0 M KOH) [9].

Inspired by the above-mentioned reports, herein we apply the widely used simple, fast and inexpensive electrodeposition technique to fabricate a low-cost, binderless and thin-layer three-dimensional (3D) binary Ni-Mo catalysts supported on titanium (Ti) surface (denoted as NiMo/Ti) followed by decoration with a very low amount of Au-crystallites (denoted as Au(NiMo)/Ti) for investigating their electrocatalytic OER performance in the alkaline medium (1.0 M NaOH).

EXPERIMENTAL

Chemicals

Titanium foil (99.7% purity) and $HAuCl_4$ (99.995%) were purchased from Sigma-Aldrich Supply. H_2SO_4 (96%), HCl (35–38%), nickel sulfate hexahydrate ($NiSO_4 \cdot 6H_2O$, >98%), sodium molybdate dihydrate ($Na_2MoO_4 \cdot 2H_2O$, >99.5%) and NaOH (98.8%) were purchased from Chempur Company. Ultra-pure water with a resistivity of 18.2 $M\Omega \cdot cm^{-1}$ was used for preparing the solutions. All chemicals were of analytical grade and used directly without further purification.

Fabrication of catalysts

The catalysts were prepared by a facile, two-step process that involves electrodeposition of the Ni-Mo layer on the surface of the titanium (Ti) electrode followed by a galvanic displacement from the Au(III)-containing solution. Prior to the deposition of the NiMo catalysts, the titanium plates were pretreated in diluted H_2SO_4 (1:1 vol) at 70°C for 3 s. NiMo catalysts were electroplated on the Ti surface (1 × 1 cm) from a bath containing 0.03 M Na_2MoO_4 along with 0.1, 0.2 and 1.0 M $NiSO_4$ in an acidic medium (1.5 M H_2SO_4 and 1 M HCl). The process of electrochemical deposition was carried out at the constant current of 0.1 and 1 A for 3 min at each current. The Au crystallites were deposited on the prepared NiMo/Ti electrodes by their immersion into 1 mM $HAuCl_4$ + 0.1 M HCl solution for 10 s. After plating, the samples were taken out, thoroughly rinsed with deionized water and air-dried at room temperature.

Characterization of catalysts

The morphology and composition of the prepared catalysts were investigated by scanning electron microscopy (SEM) using an SEM workstation SEM TM 4000 Plus (HITACHI). The metal loadings were determined by inductively coupled plasma optical emission spectrometry (ICP-OES) analysis. The ICP-OES spectra were recorded using an Optima 7000 DV spectrometer (Perkin Elmer, Waltham, MA, USA) at wavelengths of λ_{Ni} 231.604 nm, λ_{Mo} 202.031 nm and λ_{Au} 267.595 nm.

Electrochemical measurements

To investigate the electrochemical properties of our fabricated catalysts, a conventional three-electrode electrochemical cell was used and those fabricated NiMo/Ti and Au(NiMo)/Ti catalysts were employed as working electrodes, a Pt sheet was used as a counter electrode, and a calomel electrode was used as a reference. All potentials in this work were converted to the reversible hydrogen electrode (RHE) scale using the following equation (6):

$$E_{RHE} = E_{SCE} + 0.242\ V + 0.059\ V \times pH_{solution}. \quad (6)$$

Current densities were calculated using the electrode geometric area of 2 cm^2. 1 M NaOH solution was used as an alkaline medium (working electrolyte) and always deaerated by argon (Ar) for 20 min before recording each linear sweep voltammograms (LSVs). The OER polarization curves were recorded from the open circuit potential (OCP) to 2.08 V (vs RHE) at a potential scan rate of 10 $mV \cdot s^{-1}$. Polarization curves were recorded at several temperatures from 25 up to 75°C, setting the temperature with a water jacket connected to a LAUDA Alpha RA 8 thermostat. Chronoamperometry (CA) curves were recorded for 2 h at a potential of 1.83 V (vs RHE) for investigating the stability of those fabricated catalysts. All electrochemical measurements were performed with a Metrohm Autolab potentiostat (PGSTAT302) using the Electrochemical Software (Nova 2.1.4).

RESULTS AND DISCUSSION

This study presents the preparation of 3D-structured binary NiMo/Ti and ternary Au(NiMo)/Ti catalysts and their electrocatalytic performance was investigated for OER. The composition of the plating

solutions for fabricating 3D binary NiMo/Ti catalysts is listed in Table 1, and the fabrication was carried out using the electrochemical deposition method as described in the Section 'Fabrication of catalysts'. As mentioned in Table 1, the Ni^{2+}/Mo^{6+} ratio of the plating solutions was varied by changing the concentration of $NiSO_4$, while the concentration of Na_2MoO_4 was kept constant. The morphology and composition of the prepared six catalysts have been characterized by SEM and ICP-OES techniques and are presented in Fig. 1 and Table 2. Figure 1a–c shows the SEM images of the NiMo layers electrodeposited on the Ti surface and as a function of the adjacent Ni^{2+}/Mo^{6+} ratio, both the surfaces of NiMo/Ti-1 and NiMo/Ti-2 catalysts are smooth and not well-distinctive with a porous architecture Fig. (1a, b). In the case of the NiMo/Ti-3 catalyst, the lower magnification SEM image depicts the wide-ranging cedar leaf-like Ni-Mo alloy structure that grows in a large area on the Ti surface as a function of the Ni^{2+}/Mo^{6+} ratio. Those leaf-like Ni-Mo alloy architectures have been uniformly dispersed on the Ti surface and the higher magnification portraits an irregular stack of well-defined randomly distributed particles forming a cedar leaf-like structure. Figure 1f depicts the surface of Au(NiMo)/Ti-3 electrode, where Au crystallites were deposited on the prepared NiMo/Ti-3 electrode after immersing into 1 mM $HAuCl_4$ + 0.1 M HCl solution for 10 s. The mass of the elements (metal loadings) deposited onto the Ti substrate surface was determined by ICP-OES analysis (Table 2). It was found that the formed 3D binary NiMo/Ti catalysts contained ca. 83–94 wt.% of Ni, whereas those 3D ternary Au(NiMo)/Ti catalysts possessed ca. 77–88 wt.% of Ni, 6–18 wt.% of Mo and 5–6 wt.% of Au. The total metal loadings ($\mu g_{metal} cm^{-2}$) in the prepared catalysts are quite different and vary from 24 up to 106 $\mu g_{metal} cm^{-2}$.

Table 1. **Composition of the electrochemical bath**

Catalysts	Concentration in mol·dm^{-3}	
	Ni^{2+}	Mo^{6+}
NiMo/Ti-1	0.1	0.03
NiMo/Ti-2	0.2	0.03
NiMo/Ti-3	1.0	0.03

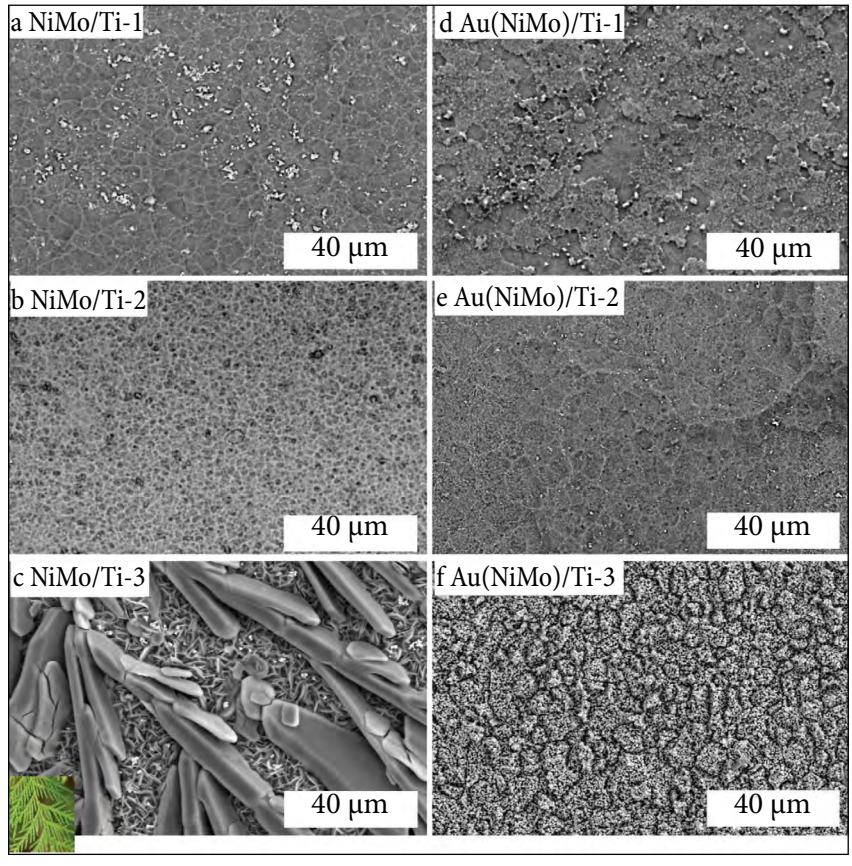

Fig. 1. SEM views of NiMo/Ti (a–c) and Au(NiMo)/Ti (d–f) catalysts mentioned in Table 2. (c) The inset represents the photo of a cedar leaf

Table 2. **The metal loading in the catalysts determined by ICP-OES analysis**

Catalyst	Ni loadings, $\mu g_{Ni} cm^{-2}$	Mo loadings, $\mu g_{Mo} cm^{-2}$	Au loadings, $\mu g_{Au} cm^{-2}$	Total metal loading, $\mu g_{metal} cm^{-2}$
NiMo/Ti-1	23.4	4.9		28.3
NiMo/Ti-2	29.6	5.3		34.9
NiMo/Ti-3	99.5	6.7		106.2
Au(NiMo)/Ti-1	18.3	4.4	1.2	23.9
Au(NiMo)/Ti-2	25.4	4.6	1.7	31.7
Au(NiMo)/Ti-3	81.4	6.0	5.2	92.6

The investigation of the electrocatalytic OER performance of the prepared catalysts was performed by recording LSVs in 1.0 M NaOH solution at a potential scan rate of 10 $mV \cdot s^{-1}$ in several temperatures from 25 up to 75°C and the potential range from the open-circuit potential (OCP) up to 2.08 V (vs RHE). Ternary Au(NiMo)/Ti-3 catalyst exhibited the highest current density (j), followed by Au(NiMo)/Ti-2 and Au(NiMo)/Ti-1. For instance, Au-decorated ternary Au(NiMo)/Ti-3, Au(NiMo)/Ti-2 and Au(NiMo)/Ti-1 catalysts reached the current densities up to 71, 37 and 21 $mA \cdot cm^{-2}$ at 25°C. On the contrary, that fabricated binary (NiMo/Ti) catalysts exhibited comparatively lower (from 1.2 to 3 times lower) current densities with a mutual comparison for OER (Fig. 2). It has been observed that the current densities increase gradually with an increase of temperature from 25 up to 75°C and for binary NiMo/Ti catalysts, j increases ca. 1.2–7.3 times higher, whereas ca. 1.3–5.1 times higher values were recorded for Au(NiMo)/Ti catalysts. Figure 3a, b depicted the current densities of 3D binary NiMo/Ti and Au-decorated ternary Au(NiMo)/Ti catalysts at 25°C, respectively.

An overpotential to reach a current density of 10 $mA \cdot cm^{-2}$ (η_{10}) was found to be similar for

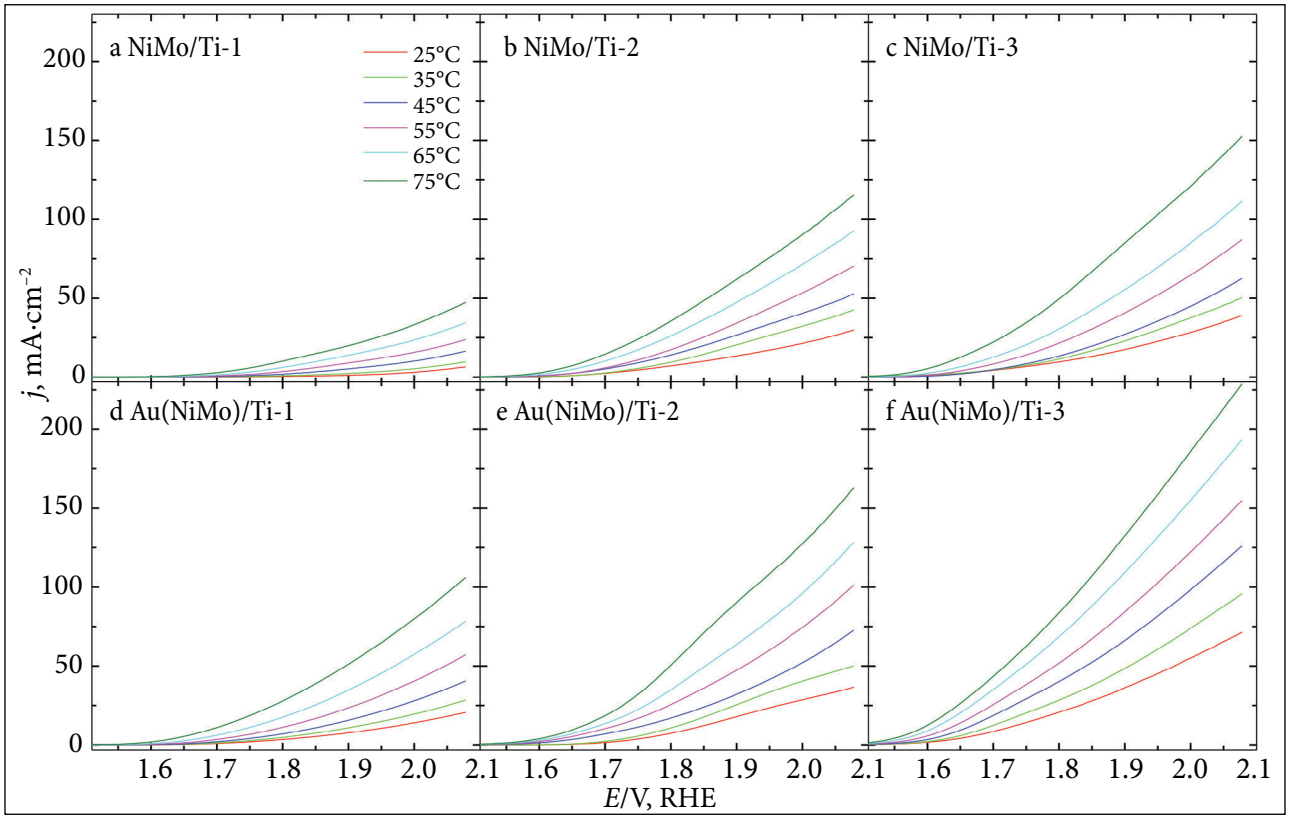

Fig. 2. OER polarization curves of 3D NiMo/Ti (a–c) and Au(NiMo)/Ti (d–f) catalysts in 1 M NaOH solution at 10 $mV \cdot s^{-1}$ potential scan rate and 25–75°C temperature range

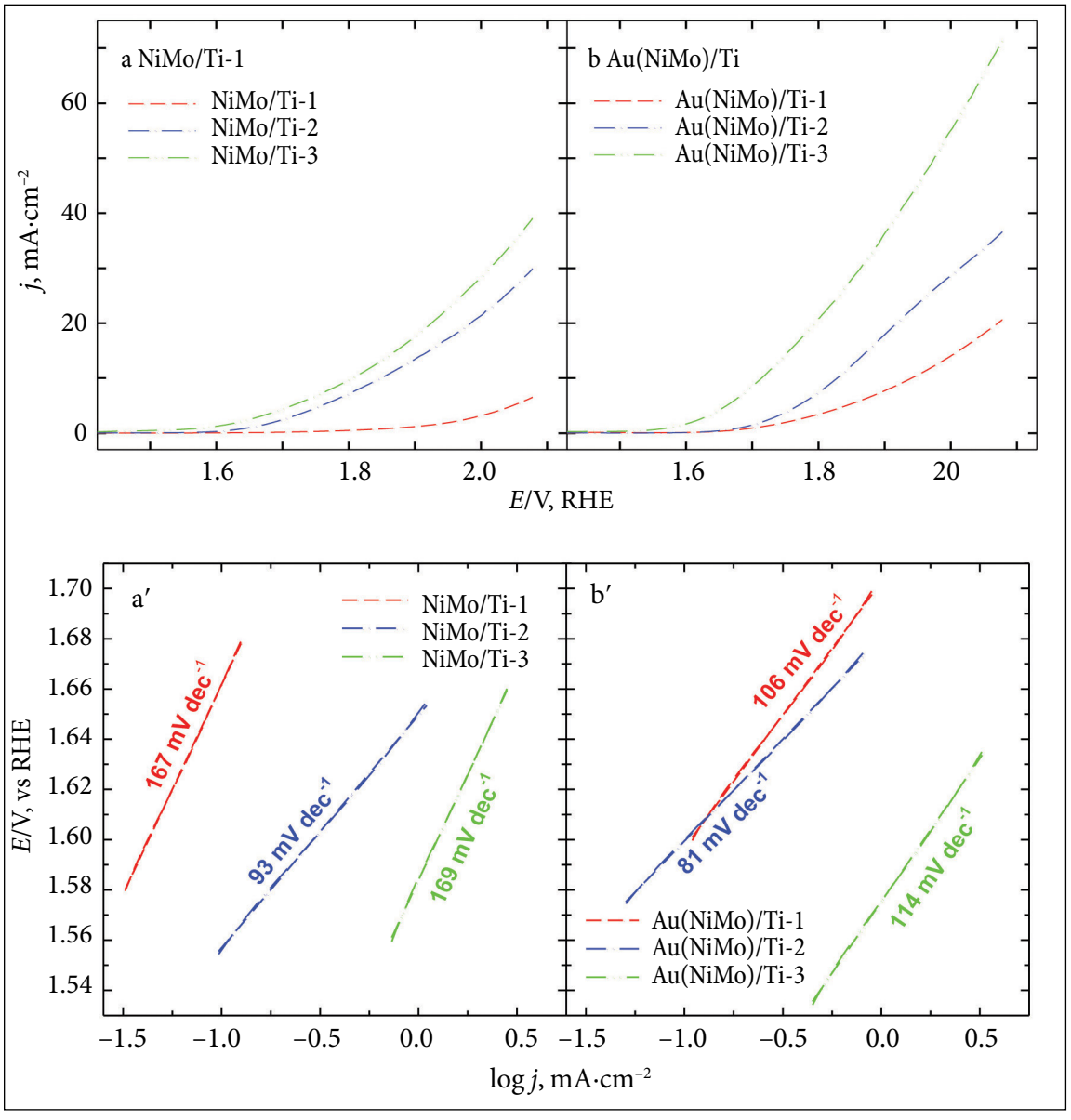

Fig. 3. OER polarization curves of 3D NiMo/Ti (a) and Au(NiMo)/Ti (b) catalysts in 1 M NaOH solution at 10 mV·s^{-1} potential scan rate and 25°C temperature and the corresponding Tafel plots (a′, b′)

Au(NiMo)/Ti-2 (600 mV), NiMo/Ti-3 (580 mV) and NiMo/Ti-2 (620 mV) and ca. 110 mV higher for Au(NiMo)/Ti-1 (710 mV) catalyst (Table 3). Au(NiMo)/Ti-3 catalyst demonstrates as the superior among all as required the lowest overpotential of 480 mV. The current density at NiMo/Ti-1 catalyst did not reach a value of 10 mA·cm^{-2} in the investigated potential range; it reached a value of only 6.52 mA·cm^{-2} at 2.08 V and 25°C. The Tafel plots were constructed by using the OER polarization curves and the resultant Tafel slopes were demonstrated in Fig. 3 (a′, b′). The Tafel slope values of 167, 93 and 169 mV·dec^{-1} were obtained for OER at NiMo/Ti-1, NiMo/Ti-2 and NiMo/Ti-3 catalysts, respectively, and the evaluated Tafel slope values for those Au-decorated ternary Au(NiMo)/Ti-1, Au(NiMo)/Ti-2 and Au(NiMo)/Ti-3 catalysts were, respectively, 106, 81 and 114 mV·dec^{-1}.

Another crucial criterion for an advanced electrode material is its electrochemical stability. To further explore and elucidate the OER activities, the durability of all six catalysts was evaluated by chronoamperometric (CA) measurements in 1 M NaOH at 1.83 V (vs RHE) for 2 h (Fig. 4). For binary NiMo/Ti catalysts, a sharp decrease in current densities was observed, while the Au(NiMo)/Ti catalysts show much higher stability for OER

Table 3. **Electrochemical performance of the tested catalysts toward OER in alkaline media**

Catalysts	j (mA·cm^{-2}) in different temperatures (°C) at 2.08 V						Tafel slope, mV·dec^{-1}	η10*, mV
	25	35	45	55	65	75		
NiMo/Ti-1	6.52	9.76	16.5	23.77	34.5	47.45	167	–
NiMo/Ti-2	29.91	42.62	52.75	70.28	92.62	115.31	93	620
NiMo/Ti-3	39.05	50.34	62.55	87.13	111.65	152.53	169	580
Au(NiMo)/Ti-1	20.63	28.46	40.59	57.16	78.34	106.14	106	710
Au(NiMo)/Ti-2	36.61	50.16	72.65	101.24	128.39	162.8	81	600
Au(NiMo)/Ti-3	71.37	95.73	126.0	154.94	193.31	228.63	114	480

* Overpotential at 10 mA·cm^{-2}.

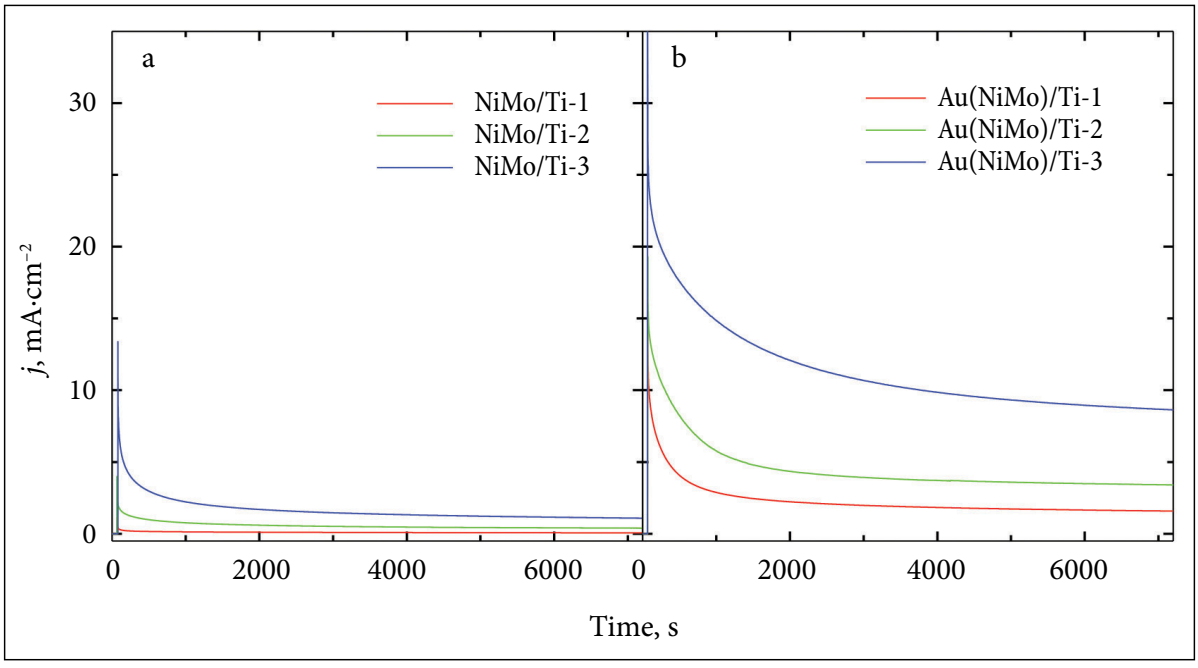

Fig. 4. Chronoamperometric data of the investigated NiMo/Ti and Au(NiMo)/Ti catalysts in 1 M NaOH solution at the potential value of 1.83 V (vs RHE), $t = 2$ h (7200 s)

in alkaline media. The CA results confirmed the result obtained by LSV analysis in terms of Au(NiMo)/Ti-3 catalyst giving the highest catalytic activity (current density) for OER (Fig. 4b). More than 2.5 times lower current density was obtained with Au(NiMo)/Ti-2 (3.39 mA·cm^{-2}) and ca. 5.5 times lower with Au(NiMo)/Ti-1 catalysts (1.57 mA·cm^{-2}) in CAs after 2 h. In the case of binary NiMo/Ti-3 coating, a comparatively lower current density was recorded (1.1 mA·cm^{-2}) along with 2.8 and more than 17 times lower value for NiMo/Ti-2 (0.39 mA·cm^{-2}) and NiMo/Ti-1 (0.06 mA·cm^{-2}) catalysts. The attained current densities after 0.5 h and after 2 h for OER are 1.3–1.8 times lower for all the prepared catalysts.

CONCLUSIONS

The binary Ni-Mo alloy coatings were successfully deposited on the Ti substrate through the electrodeposition method and subsequently decorated with a very low amount of Au-crystallites from the gold-containing solution to investigate their enhanced catalytic performance by comparing with those respective bare NiMo/Ti catalysts for oxygen evolution reaction. These fabricated binder-free electrodes exhibited a good stability, which could be ascribed to the high intrinsic activity between Ni and Mo as well as their uniformly dispersed large specific surface area. The Au(NiMo)/Ti catalysts with the low Au loadings in a range of 1.2–5.2 $\mu g_{Au} cm^{-2}$ possess ca.

1.2–3.2 times higher electrocatalytic activity towards the oxygen evolution reaction in the alkaline medium as compared to the respective binary NiMo/Ti catalysts and seem to be promising anode materials for OER. The best electrochemical activity for OER in alkaline media was obtained using Au(NiMo)/Ti-3 catalysts with the Au loading of 5.2 $\mu g_{Au} cm^{-2}$.

ACKNOWLEDGEMENTS

This research is funded by the European Social Fund under Measure No. 09.3.3-LMT-K-712-19-0138 'Development of Competences of Scientists, Other Researchers and Students through Practical Research Activities'.

Received 3 December 2022
Accepted 14 December 2022

References

1. W. Wang, M. Xu, X. Xu, W. Zhou, Z. Shao, *Angew. Chem. Int. Ed.*, **59**, 136 (2020).
2. Y. Xie, Y. Liu, Z. Yang, *Int. J. Hydrogen Energy*, **45**, 6500 (2020).
3. Y. Chen, Y. Zheng, X. Yue, S. Huang, *Int. J. Hydrogen Energy*, **45**, 8695 (2020).
4. M. A. Ashraf, C. Li, B. T. Pham, D. Zhang, *Int. J. Hydrogen Energy*, **45**, 24670 (2020).
5. M. I. Jamesh, X. Sun, *J. Energy Chem.*, **34**, 111 (2019).
6. J. Hou, Y. Wu, B. Zhang, S. Cao, Z. Li, L. Sun, *Adv. Funct. Mater.*, **29**, 1808367 (2019).
7. B. You, M. T. Tang, C. Tsai, F. Abild-Pedersen, X. Zheng, H. Li, *Adv. Mater.*, **31**, 1807001 (2019).
8. J. Song, C. Wei, Z. F. Huang, et al., *Chem. Soc. Rev.*, **49**, 2196 (2020).
9. D. Zhang, M. A. Ashraf, *Int. J. Hydrogen Energy*, **45**, 30533 (2020).
10. J. Ma, A. Cai, X. Guan, et al., *Int. J. Hydrogen Energy*, **45**, 9583 (2020).
11. C. Wei, R. R. Rao, J. Peng, et al., *Adv. Mater.*, **31**, 1806296 (2019).
12. S. L. Zhang, X. F. Lu, Z. P. Wu, D. Luan, X. W. Lou, *Angew. Chem. Int. Ed.*, **60**, 19068 (2021).
13. X. J. Cui, P. J. Ren, C. Ma, *Adv. Mater.*, **32**, 1908126 (2020).
14. J. Yin, J. Jin, M. Lu, et al., *J. Am. Chem. Soc.*, **142**, 18378 (2020).
15. L. Gao, X. Cui, C. D. Sewell, J. Li, Z. Lin, *Chem. Soc. Rev.*, **50**, 8428 (2021).
16. Y. Tian, S. Wang, E. Velasco, et al., *Iscience*, **23**, 100756 (2020).
17. W. H. Lee, M. H. Han, Y. J. Ko, B. K. Min, K. H. Chae, H. S. Oh, *Nat. Commun.*, **13**, 1 (2022).
18. C. Feng, M. B. Faheem, J. Fu, Y. Xiao, C. Li, Y. Li, *ACS Catal.*, **10**, 4019 (2020).
19. Y. Gong, J. Yao, P. Wang, Z. Li, H. Zhou, C. Xu, *Chin. J. Chem. Eng.*, **43**, 282 (2022).
20. L. Peng, J. Shen, X. Zheng, *J. Catal.*, **369**, 345 (2019).
21. H. Liang, M. Xu, E. Asselin, *J. Power Sources*, **510**, 230387 (2021).
22. C. Shuai, Z. Mo, X. Niu, et al., *J. Alloy. Compd.*, **847**, 156514 (2020).
23. F. Zheng, Z. Zhang, D. Xiang, et al., *J. Colloid Interface Sci.*, **555**, 541 (2019).
24. Y. Huang, S. L. Zhang, X. F. Lu, Z. P. Wu, D. Luan, X. W. Lou, *Angew. Chem.*, **133**, 11947 (2021).
25. X. Luo, Q. Shao, Y. Pi, X. Huang, *ACS Catal.*, **9**, 1013 (2018).
26. Y. Yang, L. Dang, M. J. Shearer, et al., *Adv. Energy Mater.*, **8**, 1703189 (2018).
27. P. Chen, J. Ye, H. Wang, L. Ouyang, M. Zhu, *J. Alloy. Compd.*, **883**, 160833 (2021).
28. H. Sun, Z. Yan, F. Liu, W. Xu, F. Cheng, J. Chen, *Adv. Mater.*, **32**, 1806326 (2020).
29. Y. Yu, J. Zhou, Z. Sun, *Adv. Funct. Mater.*, **30**, 2000570 (2020).
30. A. K. Tareen, G. S. Priyanga, K. Khan, E. Pervaiz, T. Thomas, M. Yang, *Chem. Sus. Chem.*, **12**, 3941 (2019).
31. J. Jia, M. Zhai, J. Lv, B. Zhao, H. Du, J. Zhu, *ACS Appl. Mater. Interfaces*, **10**, 30400 (2018).
32. Y. Liu, N. Ran, R. Ge, et al., *Chem. Eng. J.*, **425**, 131642 (2021).
33. S. Chen, J. Dai, F. Ren, H. Xu, Y. Du, *J. Colloid Interface Sci.*, **536**, 71 (2019).
34. C. Zhou, J. Mu, Y. F. Qi, Q. Wang, X. J. Zhao, E. C. Yang, *Int. J. Hydrogen Energy*, **44**, 8156 (2019).
35. P. Ganesan, A. Sivanantham, S. Shanmugam, *J. Mater. Chem. A*, **4**, 16394 (2016).
36. Y. Guo, T. Park, J. W. Yi, et al., *Adv. Mater.*, **31**, 1807134 (2019).
37. J. He, Z. Hu, J. Zhao, et al., *Chem. Eng. Sci.*, **243**, 116774 (2021).
38. S. Kocabas, A. Cetin, A. M. Önal, E. N. Esenturk, *J. Nanopart. Res.*, **21**, 1 (2019).
39. Y. M. Chai, X. Y. Zhang, J. H. Lin, et al., *Int. J. Hydrogen Energy*, **44**, 10156 (2019).
40. X. Zhang, Y. Li, Y. Guo, et al., *Int. J. Hydrogen Energy*, **44**, 29946 (2019).
41. G. Wu, S. Liu, G. Cheng, H. Li, Y. Liu, *Appl. Surf. Sci.*, **545**, 148975 (2021).
42. S. Xu, Y. Du, X. Liu, et al., *J. Alloy. Compd.*, **826**, 154210 (2020).
43. J. F. Qin, M. Yang, T. S. Chen, et al., *Int. J. Hydrogen Energy*, **45**, 2745 (2020).
44. M. F. Khan, A. Qurashi, *Electrochim. Acta*, **400**, 139345 (2021).
45. M. Li, Y. Zhu, H. Wang, C. Wang, N. Pinna, X. Lu, *Adv. Energy Mater.*, **9**, 1803185 (2019).
46. P. Quaino, F. Juarez, E. Santos, W. Schmickler, *Beilstein J. Nanotechnol.*, **5**, 846 (2014).

Sukomol Barua, Aldona Balčiūnaitė, Jūratė Vaičiūnienė, Loreta Tamašauskaitė-Tamašiūnaitė, Eugenijus Norkus

3D STRUKTŪROS Au(NiMo)/Ti KATALIZATORIAI EFEKTYVIAI DEGUONIES IŠSISKYRIMO REAKCIJAI

S a n t r a u k a

3D struktūros aukso-nikelio-molibdeno (Au(NiMo) katalizatorių aktyvumas tirtas deguonies išsiskyrimo reakcijai (OER). Katalizatoriai buvo nusodinti ant titano paviršiaus naudojant elektrocheminį metalų nusodinimo bei galvaninio pakeitimo metodus. Au(NiMo)/Ti katalizatoriai, kuriuose nusodinto Au kiekis yra nuo 1,2 iki 5,2 $\mu g_{Au} cm^{-2}$, pasižymėjo ~1,2–3,2 karto didesniu elektrokataliziniu aktyvumu deguonies išsiskyrimo reakcijai šarminėje terpėje, palyginti su atitinkamais NiMo/Ti katalizatoriais. Didinant temperatūrą nuo 25 iki 75 °C, deguonies išsiskyrimo srovės tankio vertės padidėja 1,2–7,3 ir ~1,3–5,1 karto, naudojant, atitinkamai, 3D NiMo/Ti ir Au(NiMo)/Ti katalizatorius.